Preventing Scars after Injury with Partial Irreversible Electroporation

Alexander Golberg[1,2], Martin Villiger[3], Saiqa Khan[4], Kyle P. Quinn[5], William C.Y. Lo[3,6], Brett E. Bouma[3,6], Martin C. Mihm, Jr.[7], William G. Austen, Jr.[4] and Martin L. Yarmush[1,8]

Preventing the formation of hypertrophic scars, especially those that are a result of major trauma or burns, would have enormous impact in the fields of regenerative and trauma medicine. In this report, we introduce a noninvasive method to prevent scarring based on nonthermal partial irreversible electroporation. Contact burn injuries in rats were treated with varying treatment parameters to optimize the treatment protocol. Scar surface area and structural properties of the scar were assessed with histology and non-invasive, longitudinal imaging with polarization-sensitive optical coherence tomography. We found that partial irreversible electroporation using 200 pulses of 250 V and 70 μs duration, delivered at 3 Hz every 20 days during a total of five therapy sessions after the initial burn injury, resulted in a 57.9% reduction of the scar area compared with untreated scars and structural features approaching those of normal skin. Unlike humans, rats do not develop hypertrophic scars. Therefore, the use of a rat animal model is the limiting factor of this work.

Journal of Investigative Dermatology (2016) ■, ■−■; doi:10.1016/j.jid.2016.06.620

INTRODUCTION

Wound care costs the U.S. health care system more than $20 billion each year, and care required to combat skin scarring represents an additional $12 billion burden (Sen et al., 2009). Hypertrophic scarring (HTS) after trauma and burn injury remains a major clinical challenge that leads to physical, aesthetic, functional, psychological, and social stresses in thousands of patients (Sen et al., 2009). Current data show that alterations in coagulation, inflammation, angiogenesis, fibroplasia, contraction, remodeling, and mechanical tension correlate with the formation of HTS (Aarabi et al., 2007; DiPietro, 2013; Rees et al., 2015; Wong et al., 2011). As yet, however, the mechanisms that induce HTS are not well understood. This gap in knowledge leads to limited clinical success in therapeutic procedures (Leventhal et al., 2006). Various techniques such as surgical excision, intralesional steroid or interferon injection, cryotherapy, laser therapy, electron-beam irradiation, mechanical compression dressing, silicone sheet application, and combinations thereof have been tested to treat scars over the years (Leventhal et al., 2006; Mofikoya et al., 2007; Rabello et al., 2014). Despite these efforts, a recent metareview shows that there are only modest improvements in the healing outcomes among all these treatments (Leventhal et al., 2006). In a parallel vein, encouraging results for tissue regeneration have been obtained using pulsed electric fields for tissue ablation in a procedure known as irreversible electroporation (IRE) (Davalos et al., 2005). IRE ablates tissue with short, pulsed electric fields that cause irreversible damage to cells by increasing the permeability of their cell membranes but spare the neighboring extracellular matrix, large blood vessels, and other accessory structures (Charpentier et al., 2010; Golberg et al., 2015a; Phillips et al., 2010; Rubinsky et al., 2007).

Inspired by recent clinical reports on the potential reduction of fibrosis in the liver after IRE instead of radiofrequency ablation (Narayanan, 2011; Rubinsky et al., 2007), and on combined bleomycin and electroporation treatment of HTS and keloids in humans (Manca et al., 2013), we set out to test the hypothesis that partial IRE (pIRE) ablation of the cells in the remodeling scar reduces scarring and diverts the wound-healing process toward scarless regeneration. This hypothesis is based on the assumption that pIRE prevents delayed myofibroblast apoptosis (Robson, 2003) and reduces the number of fibroblasts in the wound, thus creating more room for the secreted collagen to organize normally. However, pIRE of the skin is challenging, because this treatment may also lead to abnormal wound healing, contractions, and increased scarring, or even chronic wounds, if inappropriate parameters are used.

In previous work with healthy, normal skin and liver tissue, we showed that IRE preserves the extracellular matrix but

[1]*Center for Engineering in Medicine, Department of Surgery, Massachusetts General Hospital, Harvard Medical School, and the Shriners Burns Hospital, Boston, Massachusetts, USA;* [2]*Porter School of Environmental Studies, Tel Aviv University, Tel Aviv, Israel;* [3]*Wellman Center for Photomedicine, Massachusetts General Hospital and Harvard Medical School, 50 Blossom Street, Boston, Massachusetts, USA;* [4]*Department of Surgery, Division of Plastic and Reconstructive Surgery, Massachusetts General Hospital, Harvard Medical School, Boston, Massachusetts, USA;* [5]*Department of Biomedical Engineering, University of Arkansas, Fayetteville, Arkansas, USA;* [6]*Harvard-Massachusetts Institute of Technology Division of Health Sciences and Technology, Cambridge, Massachusetts, USA;* [7]*Department of Dermatology, Brigham and Women's Hospital, Harvard Medical School, Boston, MA, USA; and* [8]*Department of Biomedical Engineering, Rutgers University, Piscataway, NJ*

Correspondence: Alexander Golberg, Center for Engineering in Medicine, Department of Surgery, Massachusetts General Hospital, Harvard Medical School, and the Shriners Burns Hospital, Boston, Massachusetts, USA and Porter School of Environmental Studies, Tel Aviv University, Tel Aviv, Israel. E-mail: agolberg@tauex.tau.ac.il

Abbreviations: DOP, degree of polarization; HTS, hypertrophic scarring; IRE, irreversible electroporation; pIRE, partial irreversible electroporation; PS-OCT, polarization-sensitive optical coherence tomography; ROI, region of interest

Received 1 February 2016; revised 2 June 2016; accepted 11 June 2016; accepted manuscript published online 5 July 2016; corrected proof published online XXX

completely ablates the cells, and leads to scarless regeneration with the formation of organ appendages (Golberg et al., 2013b, 2015a). No scar or tumor formation has been observed during the 6 months of these studies. We have also developed pIRE protocols for rejuvenation of skin (Golberg et al., 2015b). In that work we showed that a single application of pIRE to normal skin in rats triggers the secretion of new collagen, the formation of additional capillaries and the proliferation of the epidermis and increases the total metabolic activity in the treated area (Golberg et al., 2015b). In addition, we also have developed methods to control fibroblast cell populations using intermittently delivered pIRE in cell cultures (Golberg et al., 2013a) and to disinfect third-degree burns with complete IRE of the infecting bacteria (Golberg et al., 2014). Here, we present a protocol for a therapeutic procedure based on intermittently delivering pIRE to burn wounds to prevent scarring.

pIRE is defined through multiple parameters such as (i) electric field strength, (ii) pulse duration, (iii) pulse number, (iv) pulse frequency, and (v) frequency of treatment delivery, which all have to be optimized to improve the therapy result. In our previous work, using a Taguchi robust experimental design approach we determined the electric field strength and the number of pulses to be the most important pIRE parameters for skin rejuvenation (Golberg et al., 2015b). Accordingly, we limited the number of tested parameters in the present study to (i) electric field strength, (ii) number of pulses, and (iii) frequency of treatment delivery. To evaluate the impact of each of these parameters and to efficiently optimize the therapy protocol, we used Taguchi LS9 orthogonal arrays for the design of experiment (Rao et al., 2008). Taguchi arrays determine the impact of individual parameters on the overall outcome of complex processes, even when several parameters are involved simultaneously (Rao et al., 2008), and are a convenient tool for biomedical engineering.

To assess the effect of pIRE on scar formation, we treated third-degree burn injuries in rats for 3 months. We used the Taguchi robust experimental design for screening and optimizing pIRE parameters. In this study we tested the applied voltages of 125 V, 250 V, and 500 V; number of pulses of 200, 400, and 800; and therapy delivery every 10 days, 20 days, or 30 days after the third-degree burn injury. The tested output parameters were scar surface area, collagen density and collagen fiber directional variance assessed by histology, and skin optical properties as detected with in vivo imaging with polarization-sensitive optical coherence tomography (PS-OCT) (Lo et al., 2016).

RESULTS

The experimental scheme and treatment schedules are shown in Figure 1. We applied the first electric field treatment (Figure 1b and c) immediately after generating the third-degree burns. Supplementary Figure S1 online presents burn injuries in equally treated validation animals at up to 1 week after the injury to show full-thickness burns. The treatments were delivered at the specified time intervals (Figure 1c) for 3 months, and the wounds were left to heal for an additional 3 months after the delivery of the last treatment. Nine combinations of the possible pIRE parameters were tested (Supplementary Table S1 online). The wound healing was monitored by visual inspection, digital photography, and with PS-OCT (Lo et al., 2016) for the entire 6 months after the burn injury.

To evaluate the impact of pIRE on the wound healing, we measured the scar surface area (Figure 2, and see Supplementary Figure S2 online) and assessed features from the analysis of PS-OCT (Figure 3, and see Supplementary

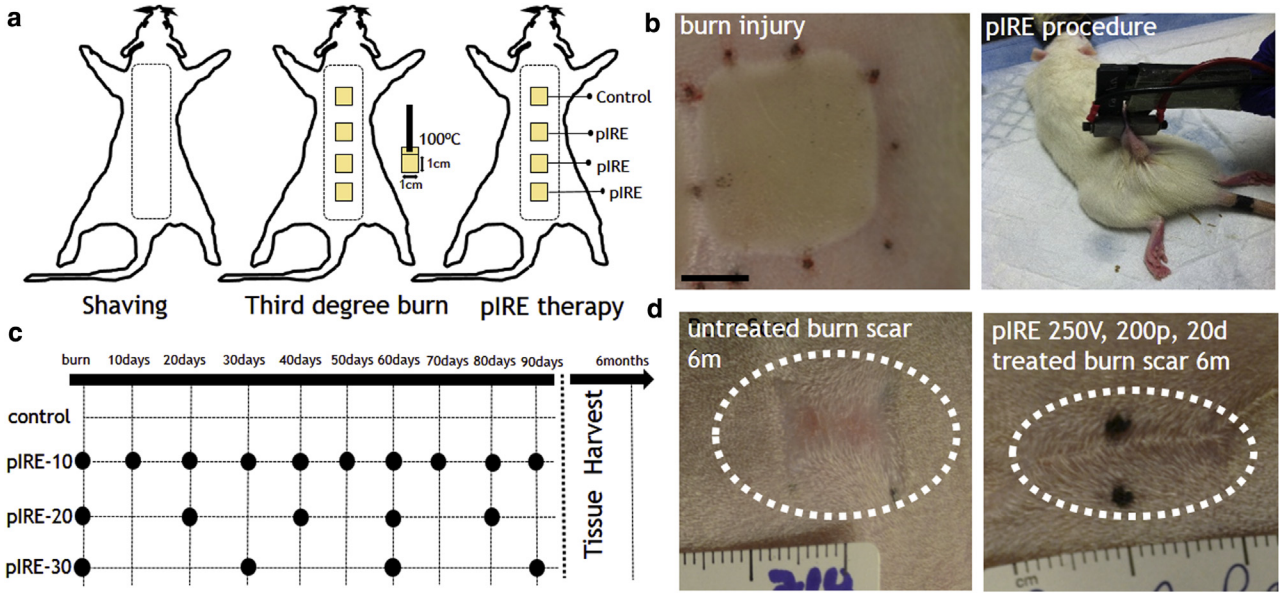

Figure 1. Partial irreversible electroporation of third-degree burns. (**a**) Schematic representation of third-degree burns on the dorsal skin of Sprague-Dawley rats. (**b**) Left panel (scale bar = 5 mm) shows the third-degree burn directly after the application of preheated brass blocks (≥95 °C) for 10 seconds. Right panel shows the pIRE procedure. (**c**) pIRE treatment schedule. (**d**) Left panel shows a typical scar resulting from untreated wound healing 6 months after the third-degree burn (n = 9). Right panel shows the wound-healing outcome on a treated lesion on the same animal after pIRE with 250 V, 200 pulses, 70 μs, 3 Hz delivered every 20 days five times after the injury. d, days; m, months; pIRE, partial irreversible electroporation.

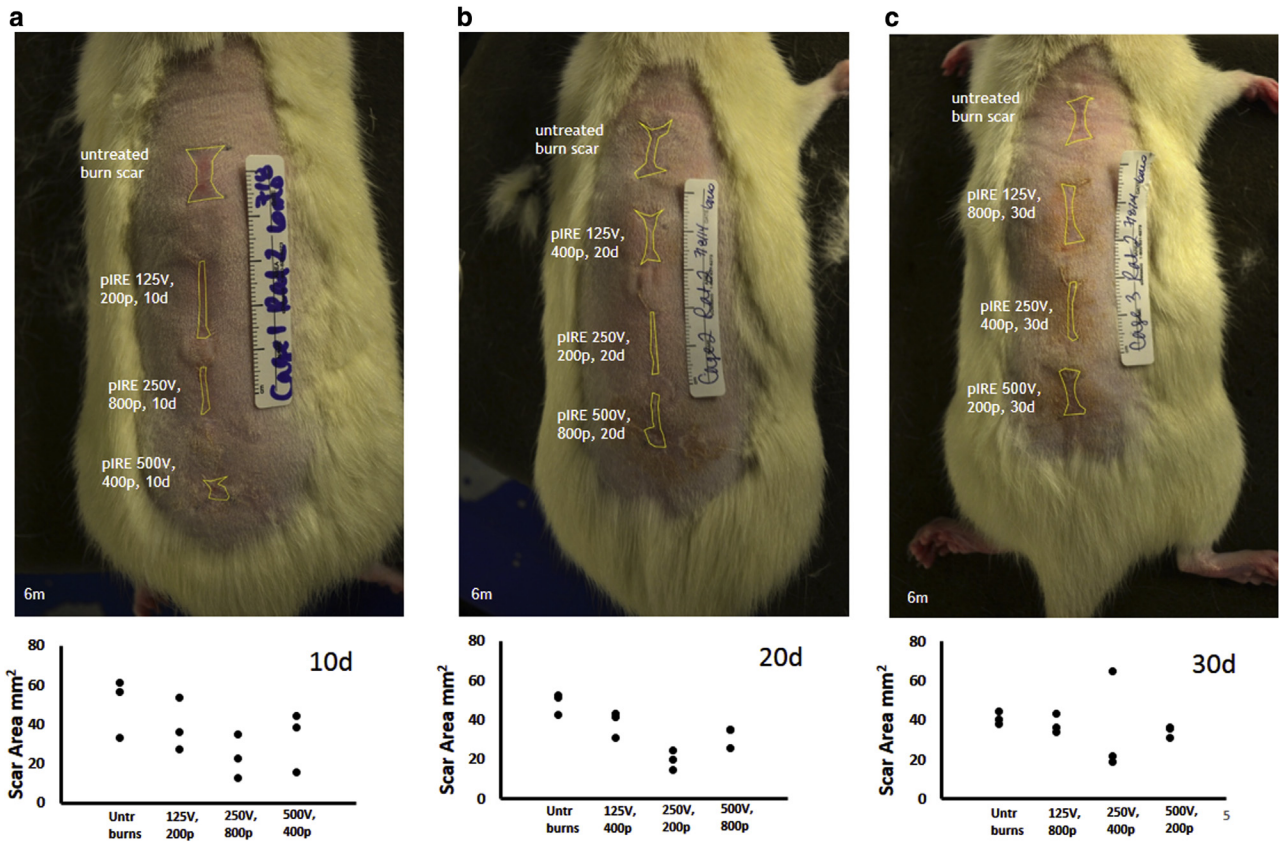

Figure 2. Appearance of treated and untreated wound healing 6 months after burn injury. (**a**–**c**) Images from representative rats from all treatment groups are shown (n = 3 animals per experimental condition). Yellow lines indicate the measured surface area of burn scars. All individual measurements are reported. d, days; m, months; p, pulses; Untr, untreated.

Figures S3, S4, and S5 online) and histology (Figure 3, and see Supplementary Figures S6, S7, and S8 online). From histological sections we measured the collagen fiber density and the fiber directional variance at the center of the original wound (Supplementary Figure S6). Fully developed scars are expected to have a higher density of fibers, paired with a lower directional variance; that is, the fibers are more organized and less intercalated than in normal skin. For PS-OCT, we performed a texture analysis of the imaged birefringence to express its homogeneity and extracted the slope of the degree of polarization (DOP) along the depth of the scar. Fully developed scars have homogenous birefringence with a slowly decreasing DOP, whereas normal skin has a very heterogeneous birefringence with a rapidly decreasing DOP. The impact of pIRE on all these features is summarized in Table 1. PS-OCT results and histology of a representative subset of the evaluated parameters appear in Figure 3. The smallest scars were observed in the group of animals treated every 20 days. (Figure 3 includes the results for in vivo PS-OCT imaging and histological analysis for this group.) Additional PS-OCT and comparison with normal skin is shown in Supplementary Figure S3.

The largest reduction in the scar size (scar size = 19.6 ± 5.1 mm^2 vs. 46.6 ± 9.1 mm^2 in the untreated burns) was achieved with 250 V and 200 pulses, applied every 20 days for 3 months after the burn injury (Figure 2b and Table 1). Five treatments were delivered for this setting. This 57.9% reduction in scar size of pIRE treated wounds compared with untreated scars was accompanied by PS-OCT (Figure 3k, u, and v, and see Supplementary Figure S3) and histological (Figure 3l, m, n, o, w, and x) features approaching those of normal skin, indicating the regenerative effect of pIRE. Wounds treated with this pIRE setting showed a homogeneity of 0.486 ± 0.027 (normal skin = 0.427 ± 0.013, untreated burns = 0.570 ± 0.027), DOP slope of 0.383 ± 0.060 (normal skin = 0.653 ± 0.097, untreated burns = 0.226 ± 0.034), fiber density of 0.821 ± 0.111 (normal skin = 0.421 ± 0.011, untreated burns = 0.796 ± 0.178), and fiber directional variance of 0.781 ± 0.028 (normal skin = 0.879 ± 0.027, untreated burns = 0.637 ± 0.085), indicating enhanced wound regeneration and resulting smaller scars (Figure 3). In addition, PS-OCT further allowed for noninvasive monitoring of the wound healing in time (see Supplementary Figures S4 and S5).

Six months after the third-degree burn injury, histopathological analysis of untreated scars showed large scars with a rectangular shape, as seen in histological cross-sections in the plane orthogonal to epidermis (Figure 3b and c). The uniformly dense dermis (with a fiber density of 0.796 ± 0.178, which is almost double the density of normal skin, 0.421 ± 0.011) (Figure 3d), overlaid with a plaque-like epidermis, featured collagen fibers that ran predominantly parallel to the surface without evidence of any normal pattern of intercalated collagen (fiber directional variance = 0.637 ± 0.085 compared with in normal skin = 0.879 ± 0.027) (Figure 3e). There were no hair follicles or other skin

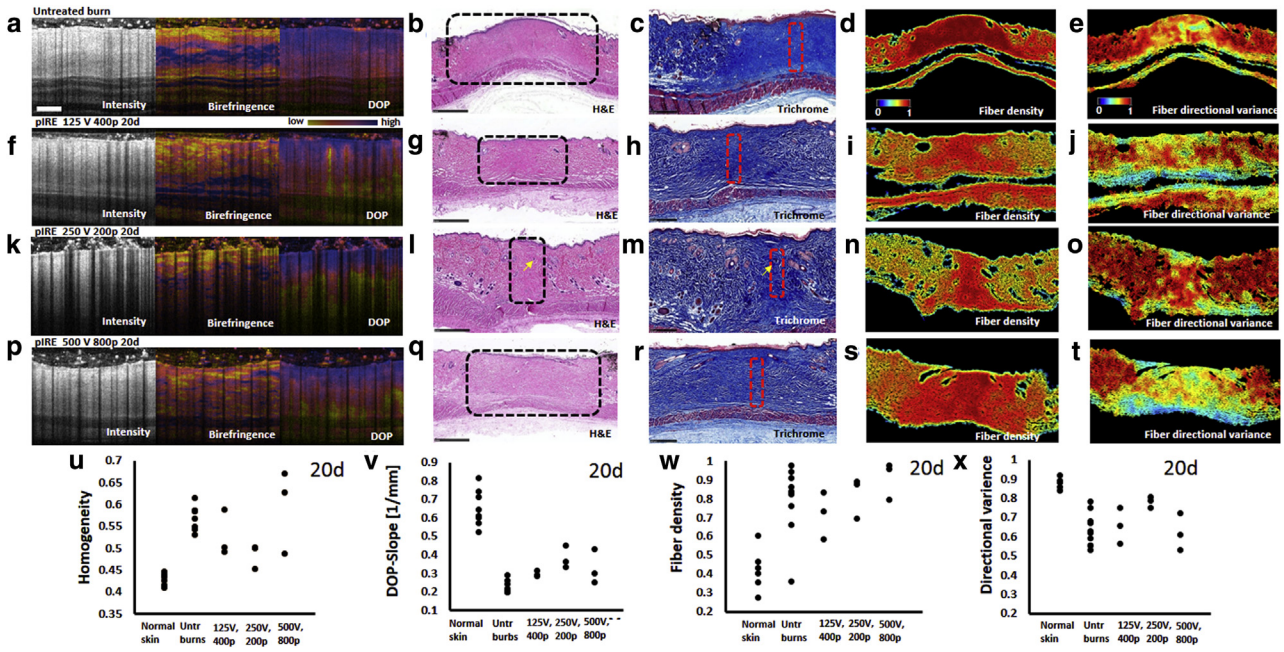

Figure 3. Skin regeneration after partial irreversible electroporation of third-degree burns 6 months after the injury. (**a**–**e**) Untreated burns (n = 9): (**a**) PS-OCT. (**b**) Histology H&E. (**c**) Histology Masson's trichrome. (**d**) Fiber density. (**e**) Fiber directional variance. (**f**–**j**) Burns treated with 125V, 400 pulses every 20 days (n = 3): (**f**) PS-OCT. (**g**) Histology H&E. (**h**) Histology Masson's trichrome. (**i**) Fiber density. (**j**) Fiber directional variance. (**k**–**o**) Burns treated with 250V, 200 pulses every 20 days (n = 3): (**k**) PS-OCT. (**l**) Histology H&E. (**m**) Histology Masson's trichrome. (**n**) Fiber density. (**o**) Fiber directional variance. (**p**–**t**) Burns treated with 500V, 800 pulses every 20 days (n = 3): (**p**) PS-OCT. (**q**) Histology H&E. (**r**) Histology Masson's trichrome. (**s**) Fiber density. (**t**) Fiber directional variance. In all pIRE protocols, pulse duration was 70 μs and pulse delivery frequency was 3 Hz. (**u**) Quantification of PS-OCT homogeneity (n = 3 for normal skin and pIRE, n = 9 for untreated burns). (**v**) Quantification of PS-OCT DOP slope (n = 3 for normal skin and pIRE, n = 9 for untreated burns). (**w**) Quantification of fiber density (n = 3 for pIRE, n = 9 for untreated controls). ROIs are shown in Supplementary Figure S6. (**x**) Quantification of fiber directional variance (n = 3 for pIRE, n = 9 for untreated controls). ROIs are shown in Supplementary Figure S6. All individual measurements are reported. ROI is shown as a black dotted line in **b**, **g**, **l** and **q** and as a red dotted line in **c**, **h**, **m** and **r**. Scale bar: **a**, **c**, **f**, **h**, **k**, **m**, **p**, **r** = 500 μm; **b**, **g**, **l**, **q** = 1 mm. d, days; DOP, degree of polarization; H&E, hematoxylin and eosin; p, pulses; pIRE, partial irreversible electroporation; PS-OCT, polarization-sensitive optical coherence tomography; ROI, region of interest.

appendages. The capillaries and venules were oriented perpendicular to surface (see Supplementary Figure S7a). In contrast, pIRE-treated wounds presented smaller scars (Figure 2) with small hair follicles in the scar area (Figure 3l and m, yellow arrows, and see Supplementary Figure S7). Different from untreated, rectangular burn scars, pIRE-treated scars featured a cross-sectional shape of a trapezoid, with the shorter base oriented toward the epidermis. Nevertheless, in the center of the treated scars the fiber density was still larger than in normal skin (0.821 ± 0.111). However, striking intercalation of collagen fibers in contrast to the linear arrangement in the untreated scars was observed (fiber directional variance in the pIRE-treated wound was 0.781 ± 0.028 compared with 0.637 ± 0.085 in the untreated burn and 0.879 ± 0.027 in normal skin). The fiber architecture was close to normal, except that the fibers were thicker than in

Table 1. The impact of the pIRE of the scar formation and properties 6 months after the third-degree burn[1]

Voltage	Number of Pulses	Treatment Frequency, days	Scar Area, mm^2	Fiber Density	Fiber Directional Variance	Homogeneity	DOP Slope, 1/mm
Normal skin			0	0.42 ± 0.05	0.88 ± 0.01	0.43 ± 0.01	0.65 ± 0.030
Untreated burn			46.6 ± 9.1	0.85 ± 0.032	0.64 ± 0.030	0.57 ± 0.009	0.22 ± 0.020
125	200	10	39.0 ± 13.4	0.87 ± 0.032	0.64 ± 0.030	0.55 ± 0.009	0.33 ± 0.011
125	400	20	38.67 ± 5.2	0.72 ± 0.021	0.66 ± 0.029	0.53 ± 0.007	0.30 ± 0.010
125	800	30	37.9 ± 4.9	0.81 ± 0.072	0.61 ± 0.054	0.55 ± 0.0031	0.29 ± 0.008
250	200	20	19.6 ± 2.5	0.82 ± 0.064	0.78 ± 0.017	0.49 ± 0.016	0.38 ± 0.035
250	400	30	35.2 ± 25.5	0.92 ± 0.027	0.70 ± 0.050	0.55 ± 0.020	0.32 ± 0.066
250	800	10	23.5 ± 11.2	0.90 ± 0.015	0.73 ± 0.024	0.55 ± 0.014	0.33 ± 0.035
500	200	30	34.4 ± 2.7	0.96 ± 0.016	0.74 ± 0.059	0.53 ± 0.042	0.36 ± 0.047
500	400	10	32.9 ± 14.9	0.85 ± 0.028	0.63 ± 0.025	0.61 ± 0.020	0.30 ± 0.032
500	800	20	31.9 ± 2.2	0.91 ± 0.058	0.62 ± 0.056	0.60 ± 0.055	0.33 ± 0.054

Abbreviation: pIRE, partial irreversible electroporation.
[1]Mean ± standard deviation are shown.

normal skin (Figure 3n, o, w, and x). The capillaries and venules in the dermis showed a close to normal, predominantly horizontal orientation (see Supplementary Figure S7b, arrows).

Using Taguchi's robust design method (Rao et al., 2008), we optimized the pIRE parameters and analyzed the significance of each of the pIRE protocol parameters (applied voltage, number of pulses, and treatment frequency) on the metrics of the wound-healing outcome (see Supplementary Materials online). Determining the role of each of the pIRE parameters is crucially important, because the results from different procedures vary substantially, and the number of all possible combinations of pIRE parameters is large. For this analysis, we computed the ratio of the outcome parameters between the pIRE-treated wound and the untreated control wound on each animal using orthogonal array Taguchi design of experiment. First, using the Taguchi ranking approach, we determined the importance of each of the treatment parameters on the change in the wound-healing parameters (see Supplementary Tables S2 and S3 online). Treatment frequency was the most important parameter for the reduction of the scar surface area. Applied voltage was the most important factor for the improvement of fiber density, fiber directional variance, and PS-OCT homogeneity of pIRE wounds compared with untreated burns. The number of pulses was the most important parameter for bringing the DOP slope of the treated wounds closer to that of normal skin. Second, we determined the best setting for each of the three pIRE parameters by individually optimizing the healing outcome, assessed with (i) scar surface area, (ii) fiber density, (iii) fiber directional variance, (iv) homogeneity, and (v) DOP slope. We found that optimum values of voltage (level 2, 250 V), number of pulses (level 1, 200 pulses), and treatment frequency (level 2, 20 days) exist for diminishing the scar size (see Supplementary Figure S8a). None of the tested parameters had a significant effect on the fiber density in the center of the analyzed region of interest (ROI) (see Supplementary Figure S8b). The optimum voltage for increasing the fiber directional variance was level 2 (250 V); the number of pulses and treatment frequency did not have a significant impact on fiber directional variance in the healed wound (see Supplementary Figure S8c). Similar results were observed for homogeneity: the optimum voltage was at level 2 (250 V), and number of pulses and treatment frequency did not play a major role in the changes of this parameter (see Supplementary Figure S8d). The optimum DOP slope was achieved with applied voltage level 2 (250 V), level 1 number of pulses (200 pulses), and slowest treatment frequency (level 3, 30 days) (see Supplementary Figure S8e). The optimum pIRE parameters to bring the wound properties closer to the values found in normal skin appear in Supplementary Table S4 online.

DISCUSSION

The complexity of the wound-healing process and our limited understanding of its mechanisms and biology led to a lack of overall progress for improved wound healing. There is a critical need for new approaches for HTS research and therapy. Complex interaction between cells, extracellular matrix, signaling factors, and environmental factors, such as oxygenation, are most often ignored in many proposed HTS therapies, which usually focus on a single target. This focus on single targets can lead to failure in clinical trials, as recently happened with transforming growth factor-β3 based therapy in 2011 (Gauglitz, 2013). Most recently, fractional laser ablation has been proposed to treat scars (Choi et al., 2014). The results from the clinical trials with this technology in burn patients are encouraging and report on textural improvement and a significant decrease of Vancouver, Patient and Observer Scar Assessment Scale, and patient scores (El-Zawahry et al., 2015; Levi et al., 2016). However, therapy depth in skin is limited because of high scattering of light in skin, causing a fundamental impediment for this technology (Preissig et al., 2012). Cryotherapy, historically limited to small scar volumes (Block et al., 2015), has improved in recent years, and up to 51% reduction of the scar size after a single treatment has been reported (Har-Shai et al., 2008). Different types of radiotherapy, such as brachytherapy, x-ray, and electron beam have been used for scar treatments; however, these technologies require special heavy equipment and need to be used carefully to avoid carcinogenesis (Block et al., 2015). In contrast to the currently used physical therapies discussed, for electroporation-based therapies, the distribution of the electric fields depends on the electrical properties of tissues, such as resistance and capacitance (Golberg et al., 2015a). Most recently, a therapy combining delivery of bleomycin with electroporation was evaluated for the treatment of HTS and keloids in humans (Manca et al., 2013). Bleomycin is currently approved only for cancer therapies and has multiple adverse effects, the major of which is pulmonary toxicity (Reinert et al., 2013).

pIRE is an HTS treatment therapy that directly affects the cell membranes, preserving the wound, without using chemicals or light. The best identified pIRE protocol includes three essential components: (i) an electric field strength corresponding to an applied voltage of 250 V across electrodes separated by 2 mm, (ii) 200 pulses, and (iii) five treatments delivered every 20 days starting at the time of injury. Using Taguchi orthogonal arrays, we have shown that this combination of parameters leads to the most significant improvement of wound regeneration after third-degree burns in terms of scar size, fiber orientation, and partial regeneration of skin appendages.

We showed here that 57.9% reduction in the size of the scar surface area compared with untreated scars, 22% increase in fiber directional variance, 15% decrease in homogeneity, and 70% increase in the DOP slope were achieved experimentally in this work with 250 V, 200 pulses, 70 μs, and 3 Hz delivered every 20 days five times after the injury. In comparison, 125 V, 200 pulses, 70 μs, and 3 Hz delivered every 10 days 10 times after the injury led to only 16.3% reduction in the scar surface area. All other treatment combinations led to outcomes within the range of 16.3% and 57.9% scar area reduction. The area of the scars was defined using manual segmentation of digital images. PS-OCT would offer the ability to automatically detect scar area and volume based on the quantitative polarization features of the imaged scars. However, the limited field of view of the system used prevented measurement of the complete scar area and volume.

We expect that additional improvement in the healing outcomes could be achieved using more precise delivery of the electric fields to the wound area. This could be achieved with flexible electrode grids to allow precise delivery of various electric fields to the different locations in the wound. An additional important issue to be addressed in following work is pain. A dense grid of electrodes could enable precise delivery of the electric fields to the upper layers of papillary dermis in humans, avoiding the exposure of large nerves in the skin. This solution could address an additional problem associated with electroporation therapies today, also observed in this study: muscle contraction (Arena et al., 2011; Golberg and Rubinsky, 2012). Further optimization of the pIRE protocol could improve additional metrics of skin regeneration, particularly the reduction of collagen fiber density in the center of the wound.

An additional problem in the field of scar therapy is the lack of understanding of the molecular mechanisms involved in scarring (Zhu et al., 2013). We are conducting ongoing research with the aim to provide a better understanding of the mechanisms resulting in improved skin regeneration after pIRE. One possible explanation is that pIRE accelerates apoptosis of fibroblasts, because delayed apoptosis in fibroblasts and fibroblast-like cells is thought to play a critical role in scar formation (Robson, 2003).

A major obstacle in preclinical research of HTS therapies is the lack of validated animal models that correspond closely to wound healing in human adults. To date, animal models of tissue regeneration and repair have focused on amphibians, rabbits, pigs, and small rodents (Ramos et al., 2008; Song et al., 2011). Our work is a first proof of concept animal study performed in small rodents, a model that obviously has limitations for studying human burns. Compared with scarring in humans, there are fundamental biological and structural limitations associated with the described protocol (Ramos et al., 2008). For example, rats have panniculus carnosus in dorsal skin, a muscle that contributes to wound contraction. Unlike humans, rats do not develop hypertrophic scars. Therefore, the use of the rat animal model is the major limitation of this work. A further limitation is the constant position of control and treated wound areas on the dorsal skin of the rats, instead of using randomized locations. The location of the wound affects the formation of scars, mediated by mechanical tension as one of the reasons (Aarabi et al., 2007). Future studies should perform location-matched comparisons of the treatment outcomes. The use of a large-animal model would also reduce the impact of self-contraction on the wound. The next major step for pIRE applied to regenerative medicine would be a first clinical trial to demonstrate the safety and efficacy of this method in humans. Translation to human patients will also require the re-optimization of the pIRE parameters for human scars to eventually enable the assessment of clinical outcomes in terms of scar appearance, pliability, tightness, neuropathic pain, and pruritus.

The pIRE approach developed in this work brings to the fore this nonthermal, chemical-free technology for HTS research and therapy. pIRE effects on tissue are very different from laser-induced tissue damage, because IRE allows for spatial and temporal control of viable cell density without any significant effect on the surrounding extracellular matrix, tissue oxygenation, and mechanical properties (Golberg et al., 2015b; Rubinsky et al., 2007). This substantively different approach for scar therapy is expected to overcome the problems that have been associated with other surgical or chemical scar therapies. The general impact of the proposed method would be very substantial both clinically and scientifically for a broad spectrum of fibrotic diseases such as HTS and heart and kidney fibrosis.

MATERIALS AND METHODS

Animal model

Female Sprague-Dawley rats (approximately 250 g, n = 18, 6 weeks old) were purchased in Charles River Laboratories (Wilmington, MA). Female animals were chosen, because in humans HTS have equal distribution between females and males (Gauglitz et al., 2011). Moreover, it was previously shown that male sex hormones potentiate, whereas female hormones reduce, burn-induced lung and gut injury in Sprague-Dawley rats, a common burn injury model (Ananthakrishnan et al., 2005). The animals were housed in cages with access to food and water ad libitum and were maintained on a 12-hour light/dark cycle in a temperature-controlled room. Pregnancy was prevented by housing the animals separate from male rats. All animal procedures were approved by the Institutional Animal Care and Use Committee of the Massachusetts General Hospital. All procedures were in accordance with the guidelines of the National Research Council.

Third-degree burn injury

Before the creation of third-degree burns, the animals (n = 3 per each treatment group) were anesthetized with isoflurane, and their fur was clipped along the dorsal surfaces. Burns were incurred by pressing the end of a preheated ($\geq$ 95 °C) brass block against the rat's dorsum for 10 seconds, resulting in a nonlethal, full-thickness, third-degree burn that measured approximately 1 cm^2 (see Supplementary Figure S1). Each burn was approximately 0.25% of the total body surface area. Four burn injuries were performed on each animal at sites separated by 2 cm along the head-to-tail axis, accounting for 1% total body surface area of total burn area. The injury closest to the head was used as control, and the other three injuries were subsequently treated with pIRE. The depth of the burn was evaluated histologically at time 0, 12 hours, and 1 week after the injury in additional (n = 3 per time point) animals (see Supplementary Figure S1).

Partial irreversible electroporation

Before pIRE treatment, animals (n = 3 per treatment group) were anesthetized with isoflurane. Their fur was clipped along the dorsal surfaces and treated with depilatory cream (Sally Hansen, Farmingdale. NY). Subsequently, burn injuries were treated with pIRE by using contact electrodes with a surface area of 1 cm^2, separated by a 2-mm gap. Square pulses of 70-μs duration at a 3-Hz repetition rate were delivered with a BTX 830 pulse generator (Harvard Apparatus Inc., Holliston, MA). Voltage, number of pulses, and treatment frequency are described in Supplementary Table S1.

Polarization-sensitive optical coherence tomography

PS-OCT was performed as reported in detail previously (Lo et al., 2016; Villiger et al., 2013). The system operated with a wavelength-swept laser source at an A-line rate of 54 kHz and a center wavelength of 1,320 nm, achieving an axial resolution of 9.4 μm. We scanned rectangular regions of 10 × 5 mm, consisting of 2,048 A-lines/image × 256 images, with a focused beam featuring a

lateral resolution of 15 μm. The lesions were covered with a thin layer of ultrasound gel as immersion liquid and apposed against a glass slide to center the superficial layers in focus. Two to three volumes were acquired for each lesion and time point, with the aim of imaging the center of the lesion. For PS-OCT, adjacent A-lines were illuminated with alternating polarization states at an angle of 90° in Stokes space, and the signal was detected with a polarization diverse receiver. Longitudinal imaging was performed on all animals monthly up to 6 months after the injury.

The data were reconstructed with spectral binning (Villiger et al., 2013), using one fifth of the spectral bandwidth, a lateral Gaussian filter with a full-width at half maximum equal to 12 adjacent A-lines, and an axial offset of 48 μm to derive depth-resolved tissue birefringence. Tissue birefringence was expressed in degrees/μm, corresponding to the amount of retardation per sample path. The DOP was evaluated independently for each spectral bin and input polarization state over the same lateral Gaussian kernel, and then averaged:

$$DOP = \frac{1}{2N}\sum_{p=1}^{2}\sum_{n=1}^{N}\frac{\sqrt{{Q_{p,n}}^2 + {U_{p,n}}^2 + {V_{p,n}}^2}}{I_{p,n}}, \qquad (1)$$

where *Q, U, V,* and *I* are the spatially averaged components of the Stokes vector, *n* denotes the spectral bin, and *p* is the input polarization state. DOP expresses the randomness of the measured polarization states in small neighborhood and scales from 0 (completely random) to unity (uniform). Close to the surface, the polarization states are usually well maintained, resulting in a DOP close to unity. As the light propagates deeper, and depending on the depolarizing properties of the tissue, the light gets increasingly depolarized, resulting in lower DOP values. The structural intensity tomograms are displayed in logarithmic scale as grayscale images. Birefringence was mapped from 0.0 to 1.2 degrees/μm with an isoluminant color map (Geissbuehler and Lasser, 2013) and overlaid with the grayscale intensity image. DOP is scaled from 0.5 to 1.0 and is rendered in the same color map. For quantitative analysis, a cylindrical region of 1-mm diameter extending from the epidermis to the subcutaneous fat was centered on the lesion at each time point. Homogeneity of the birefringence was evaluated with the "grayco-matrix" function available in the image processing toolbox in Matlab (MathWorks, Natick, MA). It was computed with an offset of five pixels in the axial direction and dividing the birefringence into 12 levels ranging from 0 to 1 degrees/μm. For the DOP slope, the DOP values were averaged at each depth across the cylinder and then fit with a straight line.

Scar area quantification

Scar surface area was quantified from digital images with ImageJ software (Schneider et al., 2012). All scar edges were traced as shown in Figure 2 and the area was quantified using a calibrated internal length standard for each image.

Histology

Specimens were harvested 6 months after the burn injury, after the last PS-OCT imaging time point. Skin samples were fixed in 10% formalin, embedded in paraffin, and cut into 7-μm sections. All samples were cut through the center of the wound along the line perpendicular to the head-to-tail axis of the animal. Sections were stained with hematoxylin and eosin and Masson's trichrome stains. Tissues were processed and stained by Wellman Center Photopathology core and the Rodent Histopathology Core at Harvard Medical School. Slides were evaluated by three individual investigators, including an experienced dermatopathologist (MCM). Color images of each entire tissue section were acquired using NanoZoomer Digital Pathology System (Nanozoomer 2.0-HT slide scanner, Hamamatsu, Hamamatsu City, Japan).

Automated image analysis of trichrome stain for fiber density and orientation

Fiber density and orientation were calculated from images of Masson's Trichrome stained sections using previously established image processing algorithms (Quinn et al., 2015). Briefly, collagen fibers were identified from the images (regions of interest are shown in Supplementary Figure S4) where the ratio of blue-to-red intensities exceeded a value of 2. Local fiber density was determined by the relative amount of collagen-positive pixels within a 50-pixel (90-μm) radius. Fiber orientation surrounding each image pixel location was also computed, and directional statistics were used to compute the local directional variance of the fibers within a 50-pixel radius. Directional variance provided a metric that was inversely proportional to the strength of fiber alignment in a preferred direction. Subregions of 300 × 700 μm corresponding to the center of the PEF-treated tissue region were defined through blinded evaluation of the original trichrome images, and the average fiber density and directional variance were computed from each subregion.

Statistical analysis

All experiments were standardized; animals of the same age were used. We used three wounds from different animals for each pIRE. Nine wounds were used as untreated burn controls. Normal skin from untreated animals was used as a positive control. Statistical analysis was performed with the statistics toolbox of MATLAB, R2009b (MathWorks, Natick, MA). Taguchi analysis was done as shown in the Supplementary Materials. Results are reported as mean ± standard deviation.

CONFLICT OF INTEREST

MV received funding for this project from the Department of Defense, Air Force Office for Scientific Research (FA9550-13-1-0068) and National Institutes of Health (P41EB015903).

ACKNOWLEDGMENTS

We acknowledge Shriners Grant #85120-BOS for the support of this study. Research in this publication was also supported in part by the Department of Defense, Air Force Office of Scientific Research under agreement number FA9550-13-1-0068 and the National Institute of Biomedical Imaging and Bioengineering of the National Institutes of Health, award P41 EB015903. We thank Dana-Farber/Harvard Cancer Center in Boston, MA, for the use of the Rodent Histopathology Core, which provided histopathology service. Dana-Farber/Harvard Cancer Center is supported in part by National Cancer Institute Cancer Center Support Grant #NIH 5 P30 CA06516. KPQ was supported by NIH R00EB017723. WCYL was supported by the Canadian Institutes of Health Research (CIHR) Doctoral Foreign Study Award.

AUTHOR CONTRIBUTIONS

AG and MY conceived study. AG, MV, WCYL, and SK did the experiments. AG, MV, KQ, MCM, WGA, BEB, and MY analyzed the data. AG, MV, and MCM wrote the paper.

SUPPLEMENTARY MATERIAL

Supplementary material is linked to the online version of the paper at www.jidonline.org, and at http://dx.doi.org/10.1016/j.jid.2016.06.620.

REFERENCES

Aarabi S, Bhatt KA, Shi Y, Paterno J, Chang EI, Loh SA, et al. Mechanical load initiates hypertrophic scar formation through decreased cellular apoptosis. FASEB J 2007;21:3250–61.

Ananthakrishnan P, Cohen DB, Xu DZ, Lu Q, Feketeova E, Deitch EA. Sex hormones modulate distant organ injury in both a trauma/hemorrhagic shock model and a burn model. Surgery 2005;137:56–65.

Arena CB, Sano MB, Rossmeisl JH, Caldwell JL, Garcia PA, Rylander M, et al. High-frequency irreversible electroporation (H-FIRE) for non-thermal ablation without muscle contraction. BioMed Eng OnLine 2011;10:102.

Block L, Gosain A, King TW. Emerging therapies for scar prevention. Adv Wound Care 2015;4:607–14.

Charpentier KP, Wolf F, Noble L, Winn B, Resnick M, Dupuy DE. Irreversible electroporation of the pancreas in swine: a pilot study. HPB (Oxford) 2010;12:348–51.

Choi JE, Oh GN, Kim JY, Seo SH, Ahn HH, Kye YC. Ablative fractional laser treatment for hypertrophic scars: comparison between Er:YAG and CO2 fractional lasers. J Dermatolog Treat 2014;25:299–303.

Davalos RV, Mir LM, Rubinsky B. Tissue ablation with irreversible electroporation. Ann Biomed Eng 2005;33:223–31.

DiPietro LA. Angiogenesis and scar formation in healing wounds. Curr Opin Rheumatol 2013;25:87–91.

El-Zawahry BM, Sobhi RM, Bassiouny DA, Tabak SA. Ablative CO2 fractional resurfacing in treatment of thermal burn scars: an open-label controlled clinical and histopathological study. J Cosmet Dermatol 2015;14:324–31.

Gauglitz GG. Management of keloids and hypertrophic scars: current and emerging options. Clin Cosmet Investig Dermatol 2013;6:103–14.

Gauglitz GG, Korting HC, Pavicic T, Ruzicka T, Jeschke MG. Hypertrophic scarring and keloids: pathomechanisms and current and emerging treatment strategies. Mol Med 2011;17:113–25.

Geissbuehler M, Lasser T. How to display data by color schemes compatible with red-green color perception deficiencies. Opt Express 2013;21:9862.

Golberg A, Bei M, Sheridan RL, Yarmush ML. Regeneration and control of human fibroblast cell density by intermittently delivered pulsed electric fields. Biotechnol Bioeng 2013a;110:1759–68.

Golberg A, Broelsch GF, Bohr S, Mihm MC, Austen WG, Albadawi H, et al. Non-thermal, pulsed electric field cell ablation: a novel tool for regenerative medicine and scarless skin regeneration. Technology 2013b;1:1–8.

Golberg A, Broelsch GF, Vecchio D, Khan S, Hamblin MR, Austen WG, et al. Pulsed electric fields for burn wound disinfection in a murine model. J Burn Care Res 2014;36:7–13.

Golberg A, Bruinsma BG, Uygun BE, Yarmush ML. Tissue heterogeneity in structure and conductivity contribute to cell survival during irreversible electroporation ablation by "electric field sinks". Sci Rep 2015a;5:8485.

Golberg A, Khan S, Belov V, Quinn KP, Albadawi H, Felix Broelsch G, et al. Skin rejuvenation with non-invasive pulsed electric fields. Sci Rep 2015b;5:10187.

Golberg A, Rubinsky B. Towards electroporation based treatment planning considering electric field induced muscle contractions. Technol Cancer Res Treat 2012;11:189–201.

Har-Shai Y, Brown W, Labbé D, Dompmartin A, Goldine I, Gil T, et al. Intralesional cryosurgery for the treatment of hypertrophic scars and keloids following aesthetic surgery: the results of a prospective observational study. Int J Low Extrem Wounds 2008;7:169–75.

Leventhal D, Furr M, Reiter D. Treatment of keloids and hypertrophic scars: a meta-analysis and review of the literature. Arch Facial Plast Surg 2006;8:362–8.

Levi B, Ibrahim A, Mathews K, Wojcik B, Gomez J, Fagan S, et al. The Use of CO2 fractional photothermolysis for the treatment of burn scars. J Burn Care Res 2016;37:106–14.

Lo WCY, Villiger M, Golberg A, Broelsch GF, Khan S, Lian CG, et al. Longitudinal, 3D in vivo imaging of collagen remodeling in murine hypertrophic scars using polarization-sensitive optical frequency domain imaging. J Invest Dermatol 2016;136:84–92.

Manca G, Pandolfi P, Gregorelli C, Cadossi M, de Terlizzi F. Treatment of keloids and hypertrophic scars with bleomycin and electroporation. Plast Reconstr Surg 2013;132:621e–30e.

Mofikoya BO, Adeyemo WL, Abdus-salam AA. Keloid and hypertrophic scars: a review of recent developments in pathogenesis and management. Nig Q J Hosp Med 2007;17:134–9.

Narayanan G. Irreversible electroporation for treatment of liver cancer. Gastroenterol Hepatol (N Y) 2011;7:313–6.

Phillips M, Maor E, Rubinsky B. Nonthermal irreversible electroporation for tissue decellularization. J Biomech Eng 2010;132:091003.

Preissig J, Hamilton K, Markus R. Current laser resurfacing technologies: a review that delves beneath the surface. Semin Plast Surg 2012;26:109–16.

Quinn KP, Golberg A, Broelsch GF, Khan S, Villiger M, Bouma B, et al. An automated image processing method to quantify collagen fibre organization within cutaneous scar tissue. Exp Dermatol 2015;24:78–80.

Rabello FB, Souza CD, Farina Júnior JA. Update on hypertrophic scar treatment. Clinics (Sao Paulo) 2014;69:565–73.

Ramos MLC, Gragnani A, Ferreira LM. Is there an ideal animal model to study hypertrophic scarring? J Burn Care Res 2008;29:363–8.

Rao RS, Kumar CG, Prakasham RS, Hobbs PJ. The Taguchi methodology as a statistical tool for biotechnological applications: a critical appraisal. Biotechnol J 2008;3:510–23.

Rees PA, Greaves NS, Baguneid M, Bayat A. Chemokines in wound healing and as potential therapeutic targets for reducing cutaneous scarring. Adv Wound Care 2015;4:687–703.

Reinert T, Serodio Da C, Baldotto R, Arthur F, Nunes P, Alves De A, et al. Bleomycin-induced lung injury. J Cancer Res 2013;480608.

Robson MC. Proliferative scarring. Surg Clin North Am 2003;83:557–69.

Rubinsky B, Onik G, Mikus P. Irreversible electroporation: a new ablation modality–clinical implications. Technol Cancer Res Treat 2007;6:37–48.

Schneider CA, Rasband WS, Eliceiri KW. NIH Image to ImageJ: 25 years of image analysis. Nat Methods 2012;9:671–5.

Sen CK, Gordillo GM, Roy S, Kirsner R, Lambert L, Hunt TK, et al. Human skin wounds: a major and snowballing threat to public health and the economy. Wound Repair Regen 2009;17:763–71.

Song F, Li B, Stocum DL. Amphibians as research models for regenerative medicine. Organogenesis 2011;6:141–50.

Villiger M, Zhang EZ, Nadkarni SK, Oh WY, Vakoc BJ, Bouma BE. Spectral binning for mitigation of polarization mode dispersion artifacts in catheter-based optical frequency domain imaging. Opt Express 2013;21:16353–69.

Wong VW, Rustad KC, Akaishi S, Sorkin M, Glotzbach JP, Januszyk M, et al. Focal adhesion kinase links mechanical force to skin fibrosis via inflammatory signaling. Nat Med 2011;18:148–52.

Zhu Z, Ding J, Shankowsky HA, Tredget EE. The molecular mechanism of hypertrophic scar. J Cell Commun Signal 2013;7:239–52.